https://doi.org/10.5194/egusphere-2025-6227
Preprint. Discussion started: 24 February 2026

Human-Driven Runoff Decline and Hydrological Drought Intensification in Semi-arid Regions in the Last 40 Years Revealed by a Hybrid Physics-Deep Learning Framework

Zhicheng Qu[1], Dongwei Liu[1] & Entao Yu [2]

[1]School of Ecology and Environment, Inner Mongolia University, Hohhot 010021, China
[2]Nansen-Zhu International Research Centre, Institute of Atmospheric Physics, Chinese Academy of Sciences, Beijing 100029, China

Correspondence to: Dongwei Liu (liudw@imu.edu.cn), Entao Yu (yuet@mail.iap.ac.cn)

Abstract. Amid accelerating global warming, the intensification of hydrological drought in semi-arid regions has become a critical threat to water security. In this study, we present an integrated framework that couples a physics-based WRF-Hydro model with a deep-learning module (LSTM-Attention) for error correction and attribution analysis. Focusing on the Xilin River Basin, a representative semi-arid catchment, this approach quantifies the relative contributions of climate change and human activities to runoff variations across interannual and intra-annual scales over the 1980–2020 period. We further systematically assess the impact of human activities on hydrological drought. Results reveal a significant runoff declining trend of -23.79×10⁴ m³/a, with an abrupt shift in 2001. During the post-shift period (2001–2020), hydrological drought frequency surged from 7.54% in the baseline period to 54.58%. Rapid warming (0.5 ℃/10a) caused sustained increase of potential evapotranspiration, while snow water equivalent decreased significantly at -1.27 mm/a; these dual effects drove the overall runoff decline. April exhibited the most pronounced runoff reduction, accounting for 58.87% of the annual decrease. In contrast, March runoff increased, primarily due to earlier snowmelt triggered by climate warming. Attribution analysis indicates that human activities were the dominant driver of runoff decline, contributing 61.04%. These activities exerted dual effects on hydrological drought: alleviating it in 29.58% of months but intensifying or triggering events in 38.34% of months. The proposed integrated framework offers a robust tool for hydrological attribution analysis and underscores the critical role of human activities in sustainable water resource management.

Keywords. Hydrological drought, Semi-arid region, Climate change, Human activities, Attribution analysis, Multiple time scales

1 Introduction

Drought — the “silent disaster” — has become a pressing global challenge (Petrova et al., 2024). Global warming is accelerating the hydrological cycle while exacerbating drought conditions in water-scarce regions. Meanwhile, escalating global water demand continues to disrupt watershed water balance (Van Loon et al., 2016). By the end of the 21st century,

https://doi.org/10.5194/egusphere-2025-6227
Preprint. Discussion started: 24 February 2026

both land area and population affected by extreme drought are projected to double (Pokhrel et al., 2021), particularly in water-scarce semi-arid regions (Cook et al., 2018). Given the growing threats to the public interest and ecosystems, attention to the mechanisms driving drought impacts has intensified worldwide (Petrova et al., 2024). It is therefore urgent to accurately identify the drivers of runoff change—an essential step toward designing targeted strategies to mitigate future societal and environmental risks (Petrova et al., 2024).

Compared to traditional empirical-statistical and conceptual water balance models, distributed hydrological models offer explicit physical mechanisms for attributing hydrological processes and effectively characterize streamflow dynamics (Hoch et al., 2023). WRF-Hydro, a widely adopted physically-based distributed hydrological model, provides a robust modeling solution through its high-resolution land surface processes and modular coupling system. However, physical models inevitably exhibit systematic biases in simulation-observation comparisons, with relatively weak performance in capturing low-flow conditions (Towler et al., 2023). With recent advances in machine learning, integrating physical hydrological models with deep learning has emerged as an effective way to improve simulation accuracy (Bhasme et al., 2022; Du and Pechlivanidis, 2025; Li et al., 2024). Among such approaches, long short-term memory (LSTM) networks better capture temporal dependencies than conventional artificial neural network (Geykli et al., 2025). By introducing an attention mechanism, LSTM-Attention (LA) further enhances the identification of key features and has demonstrated strong performance across diverse hydrological settings (Alizadeh et al., 2021; Cho and Kim, 2022).

Nevertheless, existing studies still present opportunities for improvement. Most attribution studies on runoff change focus on interannual variability, while paying insufficient attention to heterogeneous responses at intra-annual scales (Wang et al., 2025d; Zhang et al., 2025; Sun et al., 2025). In semi-arid watersheds, runoff-driving mechanisms differ markedly across characteristic periods, including snowmelt recharge, monsoon runoff generation, and agricultural irrigation. Seasonal-scale attribution analysis can help identify critical processes and dominant factors governing drought evolution. Additionally, existing physics-machine learning integrated models typically feed physical model outputs directly into deep learning algorithms for runoff prediction. This approach risks "black-boxing" physical processes, compromising model interpretability. Furthermore, human activities exert multidimensional impacts on hydrological drought—not only altering overall runoff conditions but also reshaping drought dynamics (duration, intensity, frequency). Therefore, systematic quantitative assessment of how human activities influence hydrological drought processes warrants greater attention.

This study aims to quantify the contributions of climate change and human activities to runoff variations at both interannual and seasonal scales, while systematically revealing how human activities affect hydrological drought mechanisms. To this end, we developed an integrated framework coupling physical modeling with deep learning to enhance both runoff simulation capability and attribution reliability. Unlike conventional approaches where deep learning serves as a runoff predictor, this study employs it exclusively for error correction. Specifically, LSTM-Attention functions as a "residual corrector" embedded within the physical framework. It learns and predicts residuals, then refines physical simulations through residual superposition. This strategy preserves physical mechanisms to the greatest extent while improving simulation accuracy, thereby strengthening the robustness and interpretability of attribution analysis.

https://doi.org/10.5194/egusphere-2025-6227
Preprint. Discussion started: 24 February 2026

2 Study area and data description

2.1 Study area

The Xilin River Basin (43°25′–44°39′ N, 115°02′–117°14′ E) is located in Xilingol League, central Inner Mongolia Autonomous Region (Fig. 1). Characterized by a temperate continental climate, the watershed represents a typical semi-arid region in northern China, with elevations ranging from 894 to 1609 m. According to meteorological observations, the basin experienced a mean annual precipitation of 303.64 mm/a and mean annual temperature of 3.14 ℃ during 1980–2020. The Xilin River is an inland river with a mainstream length of 175 km. In recent years, hydrological droughts and flow cessation events have occurred frequently, and water scarcity has become increasingly severe. This study focuses on the upper Xilin River Basin to investigate the drivers of hydrological regime changes. Land use is dominated by grassland, unused land, and cropland. Grasslands, primarily natural pastures, are extensively and continuously distributed across the watershed.

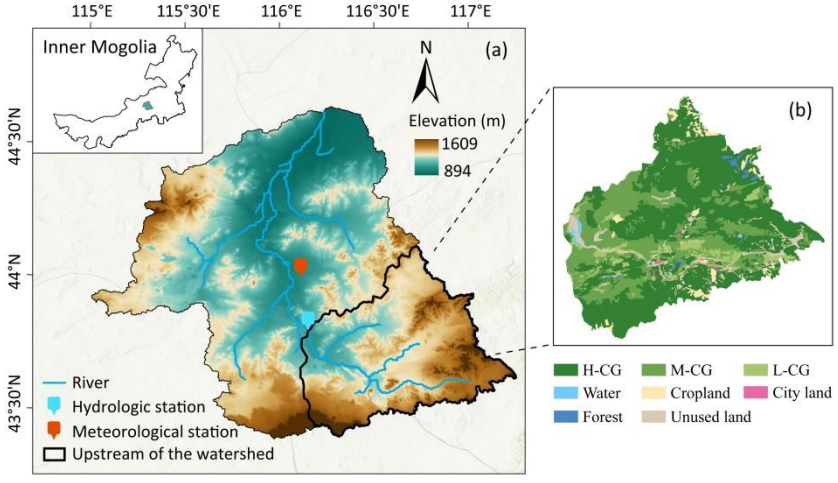

Figure 1: Location map of the Xilin River Basin. (a) Location of the study area; (b) Spatial distribution of land use types in 2000.
Note: H-GG, high-coverage grassland; M-GG, medium-coverage grassland; L-GG, low-coverage grassland.

2.2 Data

Hydrological streamflow data (1980–2020) were obtained from the Jiuquwan gauging station within the basin. Given the sparse distribution of meteorological stations in arid and semi-arid regions, which inadequately captures basin-scale climate variability, this study employed high-resolution reanalysis datasets validated against ground observations. Meteorological forcing data including temperature, precipitation, potential evapotranspiration, and snowfall (1980–2020, 0.25° × 0.25° resolution) were derived from the ERA5 reanalysis dataset produced by the European Centre for Medium-Range Weather Forecasts (ECMWF). Snow water equivalent data (1980–2020, 25 km spatial resolution) were sourced from the daily snow water equivalent/snow depth dataset for China provided by the National Cryosphere Desert Data Center (Jiang et al., 2022). Transpiration-to-evapotranspiration ratio data were obtained from the 1981–2021 transpiration-to-evapotranspiration ratio

https://doi.org/10.5194/egusphere-2025-6227
Preprint. Discussion started: 24 February 2026

dataset for China's terrestrial ecosystems (0.05 °resolution) provided by the National Ecosystem Science Data Center (Niu et al., 2020).

Land use data (1980–2020, 30 m spatial resolution) were obtained from the China Multi-period Land Use and Land Cover Remote Sensing Monitoring Dataset (CNLUCC) provided by the Resources and Environmental Science Data Platform (https://www.resdc.cn/). Human water withdrawal intensity data (1980–2020, 1 km spatial resolution) were derived from the distributed global population and water withdrawal dataset from 1960 to 2020 (Yan et al., 2022). Grazing intensity and sheep population data (1980–2024, 0.0025 ° spatial resolution) were both sourced from the National Ecosystem Science Data Center, constructed based on livestock census and satellite-derived vegetation indices (Wang et al., 2024). Local water use structure data were obtained from the Xilinhot Municipal People's Government (www.xilinhaote.gov.cn).

3 Methodology

To systematically evaluate the relative contributions of climate change and human activities to watershed hydrological drought, we developed a hybrid attribution framework integrating physically-based hydrological modeling with deep learning (Fig. 2). Based on temporal variations in precipitation and runoff, we delineated a baseline period and an altered period. The hydrological year was further divided into characteristic seasons (snowmelt period, wet season, dry season, and irrigation period) according to watershed hydrological processes. Subsequently, dynamical downscaling techniques were applied to generate high-resolution meteorological forcing data, which drove the WRF-Hydro model for parameter calibration and validation during the baseline period. Next, an LSTM-Attention residual correction module was constructed to enhance runoff simulation accuracy by learning nonlinear temporal relationships between climatic variables and systematic model biases. Then simulation-observation comparison method was employed to quantify the contributions of climate change and human activities to runoff evolution at both interannual and seasonal scales. Finally, the Standardized Runoff Index (SRI) was used to identify hydrological drought events and systematically assess the mechanisms by which human activities influence drought characteristics (duration, intensity, and frequency).

https://doi.org/10.5194/egusphere-2025-6227
Preprint. Discussion started: 24 February 2026

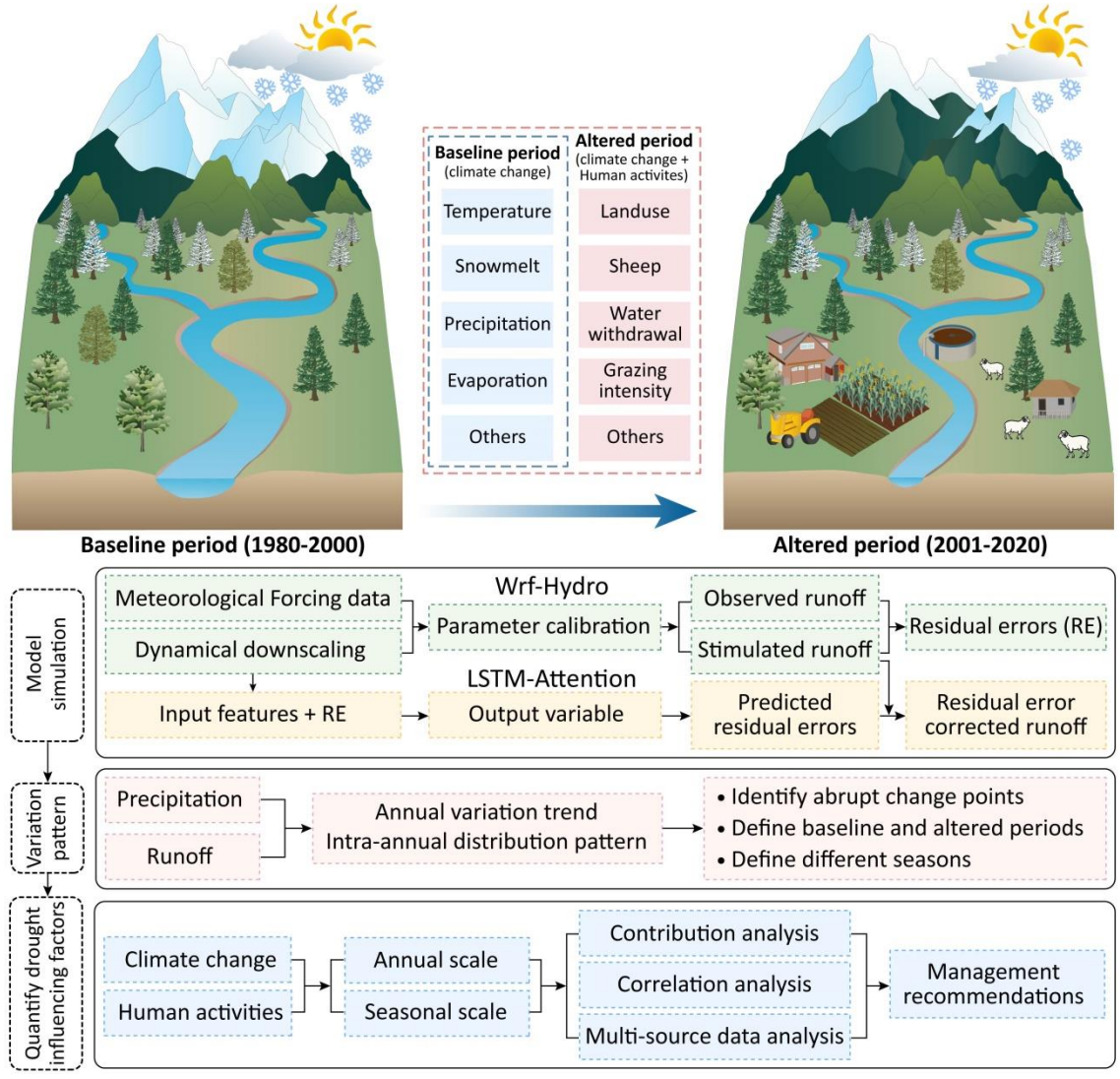

Figure 2: Technical route of this study.

3.1 Trend and Change Point Analysis

Following the hydrological series analysis methodology recommended by the World Meteorological Organization (WMO), we employed the Mann-Kendall (MK) nonparametric test to analyse trends in runoff, climate, and human activity variables during 1980–2020. Details of this method are referenced in Li et al. (Li et al., 2023). Additionally, to reduce uncertainties associated with relying on a single approach, we jointly applied the MK mutation test and Pettitt test to comprehensively identify change points in the runoff series (Chang et al., 2024).

The Mann-Kendall mutation test employs standardized statistic sequences of the forward series (UF) and backward series (UB), with confidence bounds at a given significance level serving as thresholds. When the two sequences intersect and the

https://doi.org/10.5194/egusphere-2025-6227
Preprint. Discussion started: 24 February 2026

intersection point falls within the confidence interval, the time corresponding to this intersection represents the change point. The Pettitt test identifies change points in time series based on rank statistics. At a significance level of $\alpha = 0.05$, if the maximum value of the test statistic exceeds the critical value, a significant change point is deemed to exist at that time. Both methods rely on nonparametric statistical testing, require no assumption of specific data distributions, and have been widely applied in hydrological and meteorological time series analysis (Sharma et al., 2022; Shaik and Fan, 2025).

3.2 Distributed hydrological model: WRF-Hydro

WRF-Hydro is a physics-based distributed hydrological model capable of simulating multi-scale hydrological processes at fine grid resolution, including surface runoff, subsurface flow, and channel routing (Pletzer et al., 2024; Sofokleous et al., 2023). To comprehensively represent the physical mechanisms of land surface processes, we selected the multi-parameterization land surface scheme (Noah-MP) as the land surface module for WRF-Hydro (Niu et al., 2011; Yang et al., 2011). This model can operate in coupled mode to enable two-way atmosphere-land feedback or in offline mode driven by atmospheric forcing data for distributed hydrological simulation (Tian et al., 2024). Given that this study focuses primarily on surface hydrological processes, we adopted the offline mode to run WRF-Hydro v5.1.2 for improved computational efficiency (Guo et al., 2024). The simulation domain covered the Xilin River Basin and surrounding areas, with a main grid horizontal resolution of 1 km. The WRF-Hydro sub-grid routing module employed a finer resolution of 250 m, corresponding to an aggregation factor of 4.

Meteorological forcing data were generated through dynamical downscaling of ERA5 reanalysis using the WRF model, producing meteorological fields at 12.5 km spatial resolution and 1-hour temporal resolution, including precipitation, air temperature, specific humidity, wind speed, surface pressure, and shortwave and longwave radiation. Regarding the model simulation period configuration, 1980 was designated as the spin-up period to obtain stable initial hydrological conditions. The period 1981–1985 served as the calibration period. Drawing on relevant studies in similar geographic environments (Yu et al., 2023; Guo et al., 2024), we selected parameters sensitive to hydrological processes for calibration. The period 1986–2000 served as the validation period, during which model performance was evaluated against observed runoff data. Subsequently, 2001–2020 was designated as the simulation period for hydrological process modelling. The coefficient of determination (R^2), Nash-Sutcliffe efficiency coefficient (NSE), and Kling-Gupta efficiency coefficient (KGE) were employed as comprehensive evaluation metrics. Model performance typically needs to be controlled within acceptable ranges (e.g., R^2 or NSE > 0.6) (Wang et al., 2025a) to ensure the reliability of attribution analysis.

3.3 Residual-correction model based on LSTM–Attention

To further improve the accuracy of WRF-Hydro streamflow simulations, we developed a tightly coupled hybrid framework (WH-LA) that integrates the physical model with deep learning. Unlike existing studies that employ deep learning as a direct runoff predictor to replace physical processes, this study uses LSTM-Attention as a “residual corrector.” It learns and predicts systematic biases in the physical model, improving simulation accuracy while preserving the interpretability of

https://doi.org/10.5194/egusphere-2025-6227
Preprint. Discussion started: 24 February 2026

physical mechanisms. LSTM captures temporal dependencies in hydrological processes through gating mechanisms. The Attention mechanism enhances the model's ability to identify features from high-contribution input variables by assigning different weights to climate variables and time steps. Through temporal learning and nonlinear fitting, deep learning can capture implicit relationships between climate variables and model residuals, enabling precise correction of systematic biases.

Model inputs consist of two components: (1) residual series, defined as the difference between WRF-Hydro simulated runoff and the observation; and (2) climate driving factors, including precipitation, air temperature, potential evapotranspiration, and other variables (consistent with WRF-Hydro forcing data). All input data were standardized to monthly temporal resolution. Following the standard "training-validation-simulation" partitioning approach, 1980–1996 (17 years) served as the training period, 1997–2000 (4 years) severed as the validation period, and 2001–2020 (20 years) as the simulation period.

The mathematical expression for residual correction is as follows:

$$r(t) = Q_{obs}(t) - Q_{WH}(t) \#(1)$$

Where $r(t)$ represents the residual of the hydrological model simulation, $Q_{obs}(t)$ is the observed runoff, and $Q_{\mathrm{WH}}(t)$ is the simulated runoff.

Through LSTM-Attention learning of the nonlinear temporal relationship between climate variables and residuals $r(t)$, the predicted residual $r_f(t)$ is obtained. By superimposing the predicted residual onto the original WRF-Hydro simulation results, the corrected runoff series $Q_{cor}(t)$ is derived:

$$Q_{cor}(t) = Q_{WH}(t) + r_f(t) \#(2)$$

This strategy establishes the physical model as the foundational framework and utilizes deep learning to reduce systematic biases, maximizing the preservation of physical mechanisms while enhancing simulation accuracy. This provides a more reliable runoff series for subsequent drought event identification and attribution analysis.

3.4 Drought Index

This study employed the Standardized Runoff Index (SRI) to characterize hydrological drought conditions in the watershed. SRI is based on runoff time series, uses the Gamma distribution to describe the statistical characteristics of runoff, and quantifies drought severity through normal standardization of cumulative probabilities (Li et al., 2025). We classified drought into five categories: no drought (SRI ≥ -0.5), mild drought (-1.0 < SRI < -0.5), moderate drought (-1.5 < SRI ≤ -1.0), severe drought (-2.0 < SRI ≤ -1.5), and extreme drought (SRI ≤ -2.0).

SRI not only reflects streamflow variations across different periods but also captures the lagged effects of climate change on runoff. Moreover, longer time scales can more accurately capture long-term evolution patterns and persistent change characteristics of droughts and floods (Wang et al., 2025b; Wang et al., 2025c). Therefore, this study adopted a 12-month SRI to analyze hydrological drought characteristics in the Xilin River Basin.

https://doi.org/10.5194/egusphere-2025-6227
Preprint. Discussion started: 24 February 2026

3.5 Quantitative Assessment of Climate Change and Human Activity Contributions

This study employed the simulation-observation comparison method to quantitatively assess the contributions of climate change and human activities to runoff variations. Specifically, after calibration of the hydrological model during the baseline period, we assume that the WRF-Hydro results are "perfect" simulations which represent the truly observation, and the parameters we set reflects the watershed's underlying surface characteristics and runoff generation and concentration mechanisms during that period. During the altered period, by maintaining constant parameters while updating only meteorological forcing data, the simulated runoff responds solely to climate change, whereas observed runoff is influenced by both climate change and human activities. The difference between the two represents the net effect of human activities. The specific calculation steps are as follows:

Step 1: Period delineation. Based on the change point test results from Section 3.1, the study period was divided into a baseline period and an altered period. During the baseline period, runoff changes were minimally influenced by human activities and can be neglected. During the altered period, runoff changes were jointly affected by climate change and human activities.

Step 2: Natural runoff simulation. Using the parameter set calibrated during the baseline period, the WRF-Hydro model was driven by meteorological forcing data from the altered period and corrected through LSTM-Attention residual correction to obtain the simulated runoff series for the altered period. This series represents "natural runoff" influenced only by climate change. Specifically, the total change in runoff is:

$$\Delta Q = Q_{obs,2} - Q_{obs,1} \#(3)$$

where $Q_{obs,2}$ is the multi-year average observed runoff during the altered period, and $Q_{obs,1}$ is the multi-year average observed runoff during the baseline period. The runoff change caused solely by climate change is:

$$\Delta Q_{Climate} = Q_{sim,2} - Q_{obs,1} \#(4)$$

where $Q_{sim,2}$ is the multi-year average simulated runoff during the altered period. The runoff change caused by human activities is:

$$\Delta Q_{Human} = \Delta Q - \Delta Q_{Climate} \#(5)$$

Therefore, the contribution rates of climate change ($C_{Climate}$) and human activities (C_{Human}) to runoff changes are respectively:

$$C_{Climate} = \frac{\Delta Q_{Climate}}{\Delta Q} \times 100\% \#(6)$$

$$C_{Human} = \frac{\Delta Q_{Human}}{\Delta Q} \times 100\% \#(7)$$

https://doi.org/10.5194/egusphere-2025-6227
Preprint. Discussion started: 24 February 2026

4 Result

4.1 Variation Characteristics of Climate Variables and Runoff

4.1.1 Annual Variation Trends

Fig. 3 presents the annual trends of temperature, precipitation, and runoff in the Xilin River Basin during 1980–2020. Mean annual temperature exhibited a significant increasing trend ($|Z| > 2.58$) at a rate of 0.5 ℃/10a. Annual precipitation showed a fluctuating upward trend with a growth rate of 0.15 mm/a, though this was not statistically significant ($|Z| < 1.96$). Annual runoff demonstrated a significant declining trend ($|Z| > 2.58$), decreasing at a rate of -23.79×10^4 m³/a.

Fig. 3(c–d)display the results of the MK mutation test and Pettitt test for annual runoff, respectively. Both methods identified 2001 as the critical change point year in the runoff series, with test results achieving statistical significance at the 5% level. Accordingly, 1980–2000 was designated as the baseline period. During this stage, runoff changes were primarily driven by climatic factors, with negligible human activity impacts. The period 2001–2020 was designated as the altered period, during which runoff changes were jointly influenced by both climate change and human activities. Comparing multi-year average runoff between the two periods, the baseline period averaged 1943.36×10^4 m³, which decreased to 1087.83×10^4 m³ during the altered period—a reduction of 44.03%, highlighting the acute water scarcity problem.

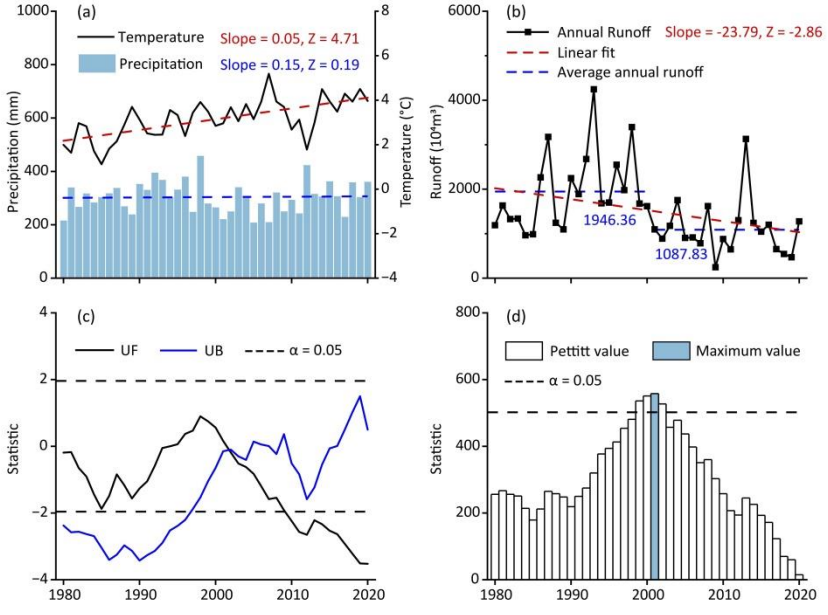

Figure 3: Interannual trends and change point identification for climate variables and runoff. (a) Trends in mean annual temperature and annual precipitation; (b) Trend in annual runoff; (c) Change point test based on the Mann-Kendall method; (d) Change point test based on the Pettitt method.

https://doi.org/10.5194/egusphere-2025-6227
Preprint. Discussion started: 24 February 2026

4.1.2 Intra-annual Distribution Pattern and Hydrological Season Division

Fig. 4 illustrates the intra-annual (monthly) distribution of precipitation and runoff in the Xilin River Basin during 1980–2020. Monthly precipitation is shown as bars (multi-year mean), and monthly runoff is summarized using box plots. Precipitation was primarily concentrated during May–September, accounting for 85.33% of the annual total. The runoff regime exhibited a bimodal distribution, with peaks occurring in April and August. April runoff, sustained by spring snowmelt recharge, reached the annual maximum (36.24% of the total). Subsequently, runoff gradually declined until concentrated rainy season precipitation generated a secondary peak. October through February of the following year constituted the dry period, during which runoff remained at low levels, with monthly runoff accounting for less than 5% of the annual total. Based on these intra-annual hydrological process characteristics, this study divided the year into four characteristic hydrological periods: early snowmelt period (March, Snow-E), when temperatures rise but snowpack has not yet undergone large-scale melting; peak snowmelt period (April, Snow-M), when rapid snowmelt generates the annual runoff peak; wet season (May–September, Rainy), characterized by concentrated rainy season precipitation and runoff generation; and dry season (October–February of the following year, Dry), characterized by sparse precipitation and low runoff. Additionally, given that the study area primarily cultivates silage corn, the critical growth period (June–August) was designated as the irrigation season (Irrigation).

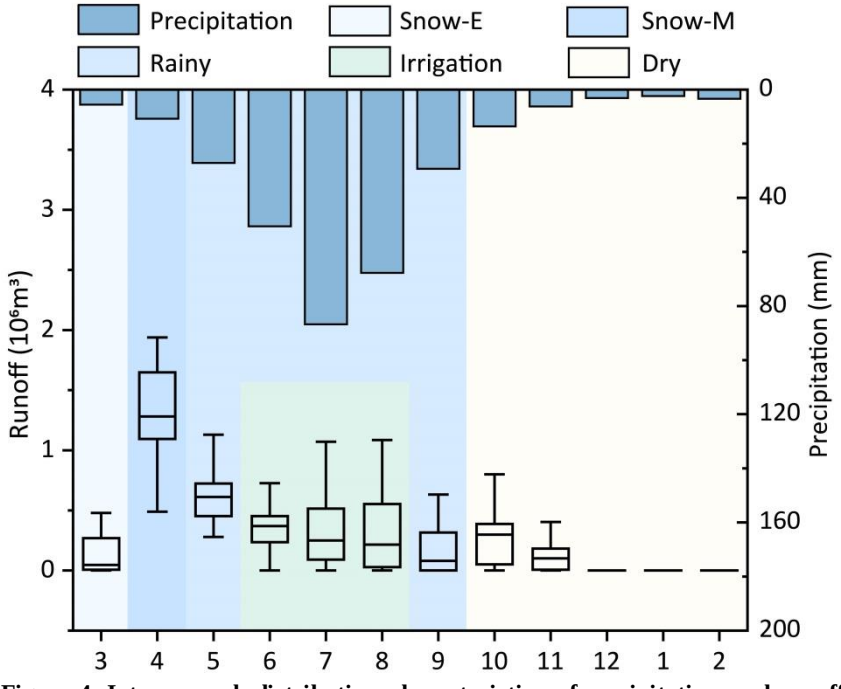

Figure 4: Intra-annual distribution characteristics of precipitation and runoff.
Note: Snow-E, early snowmelt period; Snow-M, peak snowmelt period.

https://doi.org/10.5194/egusphere-2025-6227
Preprint. Discussion started: 24 February 2026

4.2 Performance Assessment of the Integrated Model for Runoff Simulation

Fig. 5 compares the runoff simulation performance of the WRF-Hydro and WH-DL models in the study area. Overall, although the WRF-Hydro model simulated runoff agreed well with observed runoff, systematic biases persisted in peak flow simulation. In contrast, the WH-DL model produced simulated runoff with a hydrograph shape more closely resembling observations. Notably, the WH-DL model better captured peak flow characteristics during low-flow periods. To evaluate model simulation performance, the coefficient of determination (R^2), Nash-Sutcliffe efficiency coefficient (NSE), and Kling-Gupta efficiency coefficient (KGE) were employed as comprehensive metrics for parameter calibration and model validation. According to these three-evaluation metrics, the WH-DL model substantially improved runoff simulation accuracy. During the calibration period, the WH-DL model demonstrated superior performance across all three metrics, achieving values of 0.81, 0.77, and 0.70, respectively. Validation period results showed that WRF-Hydro yielded R^2, NSE, and KGE values of 0.51, 0.49, and 0.62, respectively, while the WH-DL model improved these to 0.73, 0.71, and 0.69. Overall, the WH-DL model demonstrated superior simulation performance.

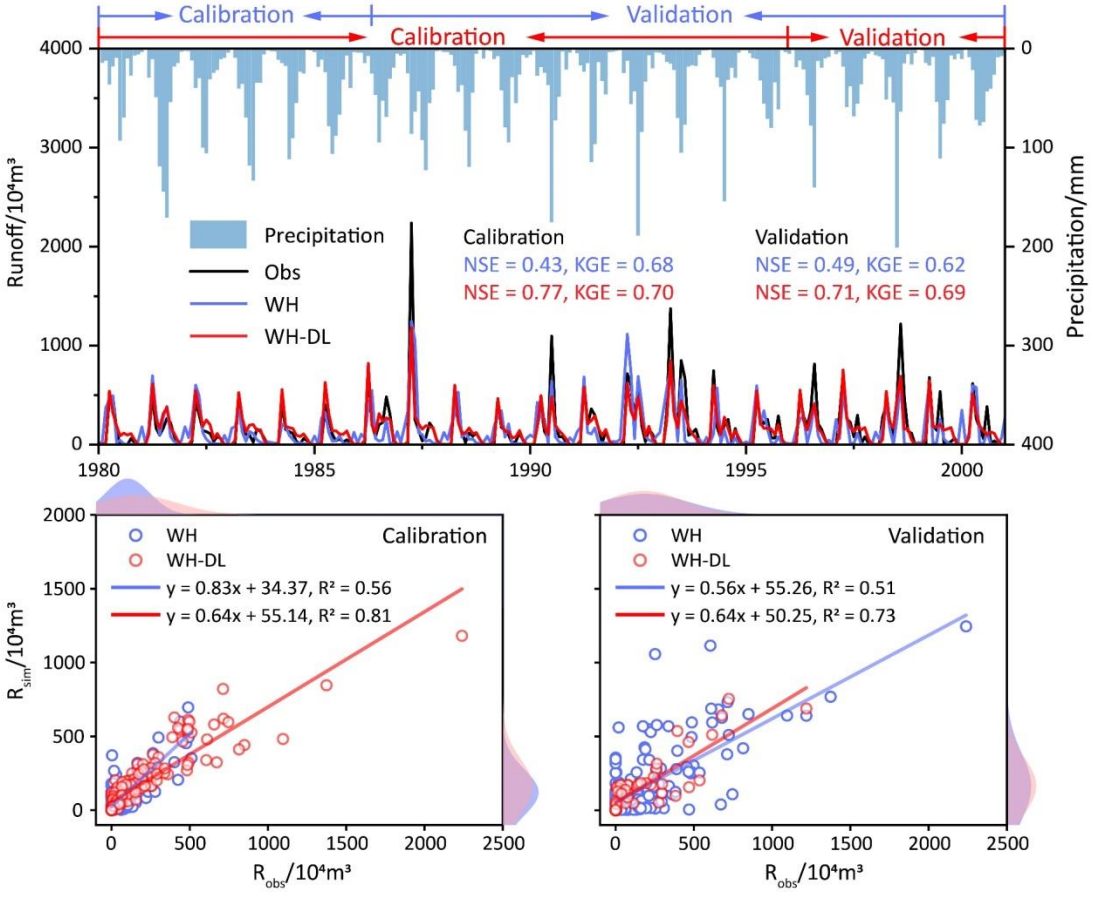

Figure 5: Comparison of runoff simulation performance between WRF-Hydro and the WH-LA integrated model.
Note: The dark blue line represents WRF-Hydro (WH) simulation results; the red line represents simulation results from WRF-Hydro combined with deep learning (WH-DL).

https://doi.org/10.5194/egusphere-2025-6227
Preprint. Discussion started: 24 February 2026

4.3 Quantitative Impacts of Climate Change and Human Activities on Runoff Variations

Fig. 6 presents the attribution analysis results based on the WH-DL model, quantitatively separating the relative contributions of climate change (blue) and human activities (red) to runoff variations at different temporal scales. Their sum represents the total change relative to observed runoff during the baseline period. As shown in Fig. 6a, at the interannual scale, human activities were the dominant driver of runoff reduction, contributing 61.04%. Further analysis revealed that during the first half of the altered period (2001-2010), climate change and human activities had comparable impacts on runoff, with contributions of -422.66×10⁴ m³/a and -477.93×10⁴ m³/a, respectively. During the second half of the altered period (2011-2020), runoff reduction attributed to human activities reached 520.31×10⁴ m³/a, with a contribution rate of approximately 65.32%.

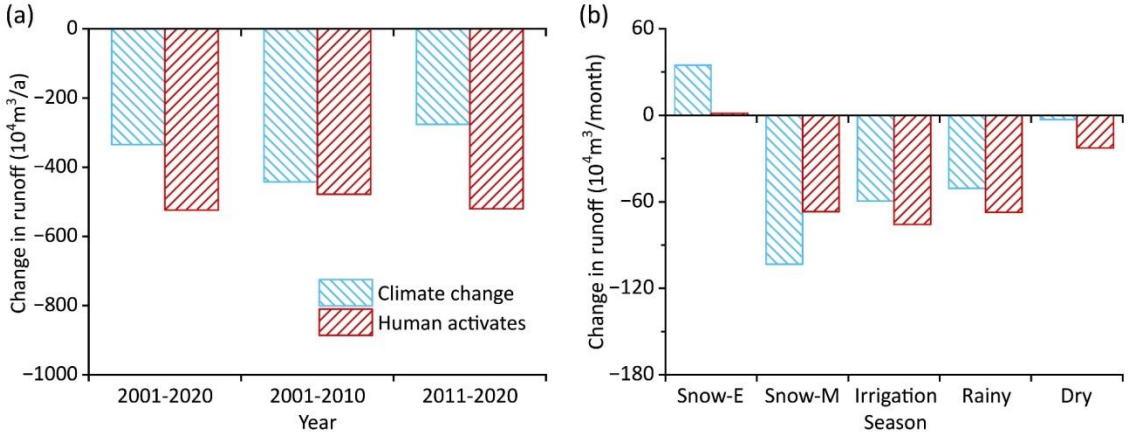

Figure 6: Impacts of climate change and human activities on runoff at annual (a) and seasonal (b) scales.

At the intra-annual scale (Fig. 6b), the Snow-M period experienced the most severe runoff reduction, contributing 58.87% to the annual runoff decline. During this period, climate change and human activities led to runoff reductions of 103.27×10⁴ m³/month and 66.83×10⁴ m³/month, respectively. Additionally, runoff changes during the Irrigation, Rainy, and Dry periods were -137.89, -115.45, and -45.61×10⁴ m³/month, respectively. Moreover, human activities contributed more than climate change across all three periods. Particularly noteworthy is that Snow-E was the only period exhibiting runoff increase, reaching 35.17×10⁴ m³/month. Further analysis revealed that climate change was the dominant driver of runoff increase during this period, contributing 34.82×10⁴ m³/month.

4.4 Different Types of Human Activity Impacts on Hydrological Drought

Based on observed and simulated runoff data from 1980–2020, we obtained variations in hydrological drought (SRI-12) and its response to human activities (Fig. 7). The observations indicate that hydrological drought intensified during the altered period compared to the baseline period. During the baseline period, the mean SRI-12 was 0.53, with only 19 months experiencing hydrological drought events (accounting for 7.54%), all of which were mild droughts. In the altered period (2001–2020), the mean SRI-12 plummeted to −0.56, with 131 drought months (54.58% of all months) and frequent

https://doi.org/10.5194/egusphere-2025-6227
Preprint. Discussion started: 24 February 2026

moderate-to-extreme drought events. Notably, two prolonged continuous drought periods emerged during the altered period in the observation, spanning June 2009–June 2012 and April 2017–July 2020, respectively. Human activities exhibited dual impacts on hydrological drought. From monthly statistics, 71 months (29.58%) showed that human activities alleviated hydrological drought, primarily concentrated during 2005–2007 and 2016–2018. Human activities intensified drought during 58 months (24.17%) and triggered drought during 34 months (14.17%). These adverse impacts primarily occurred during 2009–2011 and 2018–2020.

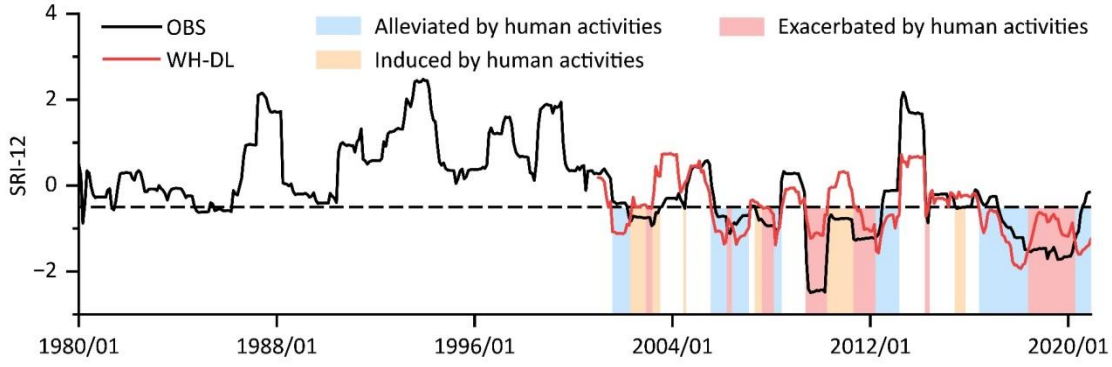

Figure 7: Three types of human activity impact patterns on hydrological drought evolution.
Note: In the figure, the black solid line represents observed SRI-12 values, while the red solid line represents simulated values. The black dashed line (SRI-12 = -0.5) indicates the drought threshold. In this study, human activity impacts on hydrological drought events were classified into three types. Blue, red, and yellow shaded areas correspond to human activities alleviating, intensifying, and triggering hydrological drought events, respectively. Specifically, when simulated values indicated drought (SRI-12 < -0.5) and observed values exceeded simulated values, this signified that human activities alleviated drought. When both observed and simulated values indicated drought events, and simulated values exceeded observed values, this signified that human activities intensified drought. When observed values indicated drought events while simulated values did not, this signified that human activities triggered drought.

5 Discussion

This study developed a hybrid attribution framework combining a physically-based distributed hydrological model with deep learning to quantitatively separate the relative contributions of climate change and human activities to runoff decline in the Xilin River across different temporal scales. In recent years, this approach has been widely adopted, with its effectiveness validated across various catchments (Kapoor and Chandra, 2026; Yao et al., 2025; Xie et al., 2026). Unlike coupling methods that "use deep learning to predict runoff," this study employs deep learning solely as an error correction module. It only corrects physical model biases without replacing the underlying physical mechanisms. This strategy enhances the accuracy of simulating different flow regimes, particularly low-flow hydrological processes, while preserving the interpretability of physical mechanisms. Consequently, it strengthens the robustness and applicability of attribution analysis. Nevertheless, the attribution framework in this study assumes that runoff variations before the change-point year were not influenced by human activities. This assumption introduces uncertainty into the quantitative analysis and may bias the calculation of contribution rates. This represents a limitation of the study.

https://doi.org/10.5194/egusphere-2025-6227
Preprint. Discussion started: 24 February 2026

5.1 Driving Mechanisms of Climate Change on Hydrological Drought

Hydrological processes are complex and driven by multiple factors. In arid/semi-arid watersheds, rising potential evapotranspiration induced by warming amplifies evaporative demand and water deficit, leading to greater water loss from the land surface (Milly and Dunne, 2016; Berghuijs et al., 2017). The relative contribution of PET becomes particularly prominent when precipitation changes are modest (Wang et al., 2022b). The Xilin River Basin's multi-year average precipitation of only 303.64 mm/a falls far below potential evapotranspiration demand (831.94 mm/a) (Qu et al., 2025), creating a persistent water deficit environment. Against this backdrop, enhanced evapotranspiration capacity reduces actually available water resources. Despite rainy season precipitation accounting for 85.33% of annual totals, its conversion efficiency to runoff remains limited, contributing only 50.89%. Precipitation does not directly convert to runoff but is primarily consumed through evapotranspiration, substantially weakening precipitation's regulatory function in alleviating drought. Additionally, temperature in the Xilin River Basin has increased significantly at 0.5℃/10a, far exceeding the concurrent global warming trend (0.2℃/10a) (Wang et al., 2022a). Rapid warming has further strengthened evapotranspiration's controlling role over hydrological processes. Although temperature and precipitation are important drivers of hydrological processes, they ranked relatively lower in the SHAP analysis. This further confirms that in water-limited semi-arid environments, water loss processes exert stronger control over runoff variations than water input processes (precipitation) (Turkeltaub and Bel, 2024).

Snowmelt, as the second-ranked contributing factor influencing hydrological processes (see Fig. S1 in the Supplement), also serves as a crucial recharge source for spring runoff. In water-scarce semi-arid environments, winter snowpack functions as a “natural reservoir”, with spring snowmelt providing substantial water replenishment to the watershed. However, under global warming, snow storage capacity has been declining significantly (Gottlieb and Mankin, 2024). In the study area, the progressive decline in snowmelt recharge capacity has directly led to severe reduction in water supply during the peak snowmelt period (see Fig. S2 in the Supplement). This corroborates the finding that runoff reduction during this period accounts for 58.87% of the total annual reduction.

On the other hand, rising temperatures have also advanced the timing of snowmelt processes (Cook et al., 2018). The early snowmelt period (March) represents the only period throughout the year exhibiting relative runoff increase, with climate change contributing the dominant role. This indicates that warming-induced earlier snowmelt provides substantial snowmelt water recharge to runoff. However, earlier snowmelt essentially represents a temporal redistribution of limited snowpack reserves rather than an increase in total volume. This also results in reduced snowmelt recharge available for later periods, as snowmelt water is dispersed to earlier time intervals. In summary, although March runoff has increased, this is primarily attributable to earlier snowmelt timing. Overall, snowpack reduction and the accompanying decline in snowmelt recharge capacity constitute critical climate driving factors exacerbating hydrological drought.

https://doi.org/10.5194/egusphere-2025-6227
Preprint. Discussion started: 24 February 2026

5.2 Watershed Hydrological Response Under Human Activity Intervention

Land use change directly manifests how human activities alter underlying surface characteristics and reshape hydrological processes. Grassland dominates the study area (accounting for more than 91% of the total area), yet it has undergone pronounced stage-wise transitions since 2000. During 2000–2010, land-use change was primarily driven by ecological restoration policies, with forest expansion being the most prominent (see Fig. S3 in the Supplement). In semi-arid regions with limited water resource carrying capacity, when vegetation ecological water demand exceeds precipitation supply capacity, rapidly expanding vegetation intensifies soil water uptake, further exacerbating water deficit (Yan et al., 2025). During 2011–2020, agricultural development and urban construction accelerated. Although these two land types represented small proportions (totaling approximately 3–4%), they were predominantly distributed near river channels. This facilitated more convenient and frequent channel water diversion and shallow groundwater extraction activities, directly reducing channel runoff. Additionally, local agriculture focuses primarily on silage corn cultivation, with crops requiring substantial irrigation water during the growing period. This corroborates the finding that human activities contribute most significantly to runoff reduction during the irrigation season. Furthermore, from the local water use structure perspective, irrigation water use and domestic water use accounted for 53.5% and 27.7% of total water consumption, respectively. Agricultural irrigation exhibits characteristics of high water consumption and high evapotranspiration. It directly extracts surface water and shallow groundwater to meet crop demands, while large volumes of water are consumed through farmland evapotranspiration after irrigation, with minimal return to channels. Domestic water use weakens runoff recharge through continuous water extraction and urban expansion (Mcdonald et al., 2011). Moreover, with population growth and rising living standards, water demand will continue to increase.

In addition, human water withdrawal intensity, sheep population, and grazing intensity have increased significantly over the past ~40 years (see Fig. S4 in the Supplement). Sustained intensification of human water withdrawal directly reduces channel runoff and indirectly alters runoff recharge mechanisms by affecting surface water-groundwater exchange processes. With continuous growth in agricultural irrigation, domestic water use, and livestock drinking water demands, extraction intensity of surface water and shallow groundwater has intensified, further reducing channel runoff recharge. Furthermore, improper grazing practices lead to vegetation degradation and increased bare soil area. This exacerbates soil moisture evapotranspiration, reduces soil water storage, and affects runoff generation (An et al., 2019). Additionally, livestock manure and urine elevate soil nitrogen and phosphorus content, reducing soil water retention capacity (Zhou et al., 2024). Moreover, heavily grazed grassland areas typically harbor higher abundances of soil insects (such as beetles). The biological channels created by their burrowing activities enhance soil infiltration capacity and reduce channel runoff concentration. In summary, to reduce hydrological drought risk, measures such as establishing riparian fencing and optimizing grazing practices can be implemented (Chen et al., 2022; Shi et al., 2022).

https://doi.org/10.5194/egusphere-2025-6227
Preprint. Discussion started: 24 February 2026

6 Conclusions

This study presents an integrated modeling framework coupling physics-based WRF-Hydro model with deep learning to investigate the hydrological drought variations in the Xilin River Basin and their dual climate-human driving mechanisms. Deep learning, embedded as an "error corrector" within the framework, enhanced runoff simulation accuracy. In particular, it improved the capacity to capture low-flow processes and peak characteristics, thereby strengthening the reliability of hydrological drought attribution.

During 1980–2020, annual runoff in the Xilin River declined significantly, with an abrupt shift occurring in 2001. In subsequent the altered period, hydrological drought frequency, duration, and intensity all intensified. In seasonal scale, runoff reduction during the peak snowmelt period was most pronounced, contributing 58.87% to total reduction. In contrast, during the early snowmelt period, runoff increased relative to the baseline period due to earlier snowmelt induced by warming. Attribution analysis highlights potential evapotranspiration and snowmelt as key climatic factors influencing runoff. Local temperature rise far beyond the global average, causing persistent evapotranspiration increase under a background of relatively stable precipitation changes, indicating evapotranspiration as the main climatic driver of long-term runoff decline. Meanwhile, snow water decreased significantly at -1.27 mm/a, causing substantial spring runoff reduction due to declining snowmelt recharge. Human activities, on the other hand, played the dominant role in runoff reduction, explaining 61.04% of the runoff drop and exacerbated drought risk through multiple pathways, including sustained increase in water withdrawal intensity, overgrazing disruption on watershed water balance and so on. At the same time, rapid land use transformation, such as vegetation restoration that enhanced transpiration consumption, coupled with expansion in cropland and built-up areas that accelerated water consumption, further weakened surface-groundwater recharge and concentration processes, ultimately intensified hydrological drought.

In summary, water resource security in the Xilin River Basin is under crucial threat. The integrated modeling framework proposed in this study provides a robust tool for water planning in semi-arid regions, building confidence in addressing challenges of climate change and human activities on hydrological drought in water-stressed areas.

Code and data availability

The WRF-Hydro model is available from GitHub (https://github.com/NCAR/wrf_hydro_nwm_public.git). ERA5-Land data were obtained from the Copernicus Climate Data Store (DOI: 10.24381/cds.e2161bac). The LSTM-Attention algorithm and the associated dataset used in this study are available at https://github.com/Wir2019/Climate-Driven-Runoff-Modeling-LSTM-Attention.git. Snow water equivalent data are available from the National Earth System Science Data Center, National Science & Technology Infrastructure of China (DOI: 10.12041/geodata.214988958860999.ver1.db). The transpiration-to-evapotranspiration ratio (T/ET) dataset for China's terrestrial ecosystems is available at DOI: 10.17605/OSF.IO/MERZN. Land-use data were obtained from the Data Center for Resources and Environmental Sciences, Chinese Academy of Sciences (DOI: 10.12078/2018070201). Human water-withdrawal intensity data are available at

https://doi.org/10.5194/egusphere-2025-6227
Preprint. Discussion started: 24 February 2026

https://doi.org/10.6084/m9.figshare.19387406. Grazing intensity and sheep stock data are available at DOI: 10.6084/m9.figshare.26195684.v3. Local water-use structure data were obtained from publicly available records of the Xilinhot Municipal People's Government (www.xilinhaote.gov.cn, accessed on 10 June 2025).

Author contributions

Zhicheng Qu: Writing – original draft, Visualization, Software, Methodology, Conceptualization. Dongwei Liu: Writing – review & editing, Supervision, Investigation, Conceptualization. Entao Yu: Writing – review & editing, Methodology.

Competing interests

The authors declare that they have no conflict of interest.

Data availability

Data will be made available on request.

Financial support

This research is funded by Project of Key Laboratory of River and Lake in Inner Mongolia Autonomous Region (2025KYPT0020).

References

Alizadeh, B., Ghaderi Bafti, A., Kamangir, H., Zhang, Y., Wright, D. B., and Franz, K. J.: A novel attention-based LSTM cell post-processor coupled with bayesian optimization for streamflow prediction, Journal of Hydrology, 601, 126526, https://doi.org/10.1016/j.jhydrol.2021.126526, 2021.

An, T., Xu, M., Zhang, T., Yu, C., Li, Y., Chen, N., Zu, J., Li, J., Zhu, J., Sun, Y., Zhao, T., and Yu, G.: Grazing alters environmental control mechanisms of evapotranspiration in an alpine meadow of the Tibetan Plateau, Journal of Plant Ecology, 12, 834-845, https://doi.org/10.1093/jpe/rtz021, 2019.

Berghuijs, W. R., Larsen, J. R., van Emmerik, T. H. M., and Woods, R. A.: A Global Assessment of Runoff Sensitivity to Changes in Precipitation, Potential Evaporation, and Other Factors, Water Resources Research, 53, 8475-8486, https://doi.org/10.1002/2017wr021593, 2017.

https://doi.org/10.5194/egusphere-2025-6227
Preprint. Discussion started: 24 February 2026

Bhasme, P., Vagadiya, J., and Bhatia, U.: Enhancing predictive skills in physically-consistent way: Physics Informed Machine Learning for hydrological processes, Journal of Hydrology, 615, 128618, https://doi.org/10.1016/j.jhydrol.2022.128618, 2022.

Chang, Y., Ding, Y., Zhang, S., Zhao, Q., Jin, Z., Qin, J., and Shangguan, D.: Quantifying the response of runoff to glacier shrinkage and permafrost degradation in a typical cryospheric basin on the Tibetan Plateau, CATENA, 242, 108124, https://doi.org/10.1016/j.catena.2024.108124, 2024.

Chen, C., Zou, X., Singh, A. K., Zhu, X., Jiang, X., Wu, J., and Liu, W.: Effects of grazing exclusion on soil infiltrability and preferential flow in savannah livestock grazing systems, Land Degradation & Development, 33, 3010-3022, https://doi.org/10.1002/ldr.4368, 2022.

Cho, K. and Kim, Y.: Improving streamflow prediction in the WRF-Hydro model with LSTM networks, Journal of Hydrology, 605, 127297, https://doi.org/10.1016/j.jhydrol.2021.127297, 2022.

Cook, B. I., Mankin, J. S., and Anchukaitis, K. J.: Climate Change and Drought: From Past to Future, Current Climate Change Reports, 4, 164-179, https://doi.org/10.1007/s40641-018-0093-2, 2018.

Du, Y. and Pechlivanidis, I. G.: Hybrid approaches enhance hydrological model usability for local streamflow prediction, Communications Earth & Environment, 6, 334, https://doi.org/10.1038/s43247-025-02324-y, 2025.

Geykli, A. N., Gul, E., Naderi, S., Rasouli, K., and Nikoo, M. R.: Exploring the attributive impacts of climate and land use changes on streamflow in an urbanized watershed by deep learning and physically based modeling, Journal of Cleaner Production, 523, 146433, https://doi.org/10.1016/j.jclepro.2025.146433, 2025.

Gottlieb, A. R. and Mankin, J. S.: Evidence of human influence on Northern Hemisphere snow loss, Nature, 625, 293-300, https://doi.org/10.1038/s41586-023-06794-y, 2024.

Guo, S., Tian, L., Chen, S., Liang, J., Tian, J., Cao, B., Wang, X., and He, C.: Analysis of effects of vegetation cover and elevation on water yield in an alpine basin of the Qilian Mountains in Northwest China by integrating the WRF-Hydro and Budyko framework, Journal of Hydrology, 629, 130580, https://doi.org/10.1016/j.jhydrol.2023.130580, 2024.

Hoch, J. M., Sutanudjaja, E. H., Wanders, N., van Beek, R. L. P. H., and Bierkens, M. F. P.: Hyper-resolution PCR-GLOBWB: opportunities and challenges from refining model spatial resolution to 1 km over the European continent, Hydrol. Earth Syst. Sci., 27, 1383-1401, https://doi.org/10.5194/hess-27-1383-2023, 2023.

Jiang, L., Yang, J., Zhang, C., Wu, S., Li, Z., Dai, L., Li, X., and Qiu, Y.: Daily snow water equivalent product with SMMR, SSM/I and SSMIS from 1980 to 2020 over China, Big Earth Data, 6, 420-434, https://doi.org/10.1080/20964471.2022.2032998, 2022.

Kapoor, A. and Chandra, R.: QDeepGR4J: Quantile-based ensemble of deep learning and GR4J hybrid rainfall-runoff models for extreme flow prediction with uncertainty quantification, Journal of Hydrology, 664, 134434, https://doi.org/10.1016/j.jhydrol.2025.134434, 2026.

https://doi.org/10.5194/egusphere-2025-6227
Preprint. Discussion started: 24 February 2026

Li, B., Sun, T., Tian, F., Mahmut, T., Li, Q., and Ni, G.: Hybrid hydrological modeling for large alpine basins: a semi-distributed approach, Hydrology and Earth System Sciences, 28, 4521-4538, https://doi.org/10.5194/hess-28-4521-2024, 2024.

Li, C., Hao, J., Zhang, G., Fang, H., Wang, Y., and Lu, H.: Runoff variations affected by climate change and human activities in Yarlung Zangbo River, southeastern Tibetan Plateau, CATENA, 230, 107184, https://doi.org/10.1016/j.catena.2023.107184, 2023.

Li, X., Zhang, X., Hong, X., Ni, Z., and Jiang, C.: A novel approach for the estimation of hydrological drought index incorporating precipitation-runoff relationship, Journal of Hydrology, 653, 132734, https://doi.org/10.1016/j.jhydrol.2025.132734, 2025.

McDonald, R. I., Green, P., Balk, D., Fekete, B. M., Revenga, C., Todd, M., and Montgomery, M.: Urban growth, climate change, and freshwater availability, Proceedings of the National Academy of Sciences, 108, 6312-6317, https://doi.org/10.1073/pnas.1011615108, 2011.

Milly, P. C. D. and Dunne, K. A.: Potential evapotranspiration and continental drying, Nature Climate Change, 6, 946-949, https://doi.org/10.1038/nclimate3046, 2016.

Niu, G., Yang, Z., Mitchell, K. E., Chen, F., Ek, M. B., Barlage, M., Kumar, A., Manning, K., Niyogi, D., Rosero, E., Tewari, M., and Xia, Y.: The community Noah land surface model with multiparameterization options (Noah-MP): 1. Model description and evaluation with local-scale measurements, Journal of Geophysical Research-Atmospheres, 116, https://doi.org/10.1029/2010jd015139, 2011.

Niu, Z., He, H., Zhu, G., Ren, X., Zhang, L., and Zhang, K.: A spatial-temporal continuous dataset of the transpiration to evapotranspiration ratio in China from 1981–2015, Scientific Data, 7, 369, https://doi.org/10.1038/s41597-020-00693-x, 2020.

Petrova, I. Y., Miralles, D. G., Brient, F., Donat, M. G., Min, S.-K., Kim, Y.-H., and Bador, M.: Observation-constrained projections reveal longer-than-expected dry spells, Nature, 633, 594-600, https://doi.org/10.1038/s41586-024-07887-y, 2024.

Pletzer, T., Conway, J. P., Cullen, N. J., Eidhammer, T., and Katurji, M.: The application and modification of WRF-Hydro/Glacier to a cold-based Antarctic glacier, Hydrology and Earth System Sciences, 28, 459-478, https://doi.org/10.5194/hess-28-459-2024, 2024.

Pokhrel, Y., Felfelani, F., Satoh, Y., Boulange, J., Burek, P., Gädeke, A., Gerten, D., Gosling, S. N., Grillakis, M., Gudmundsson, L., Hanasaki, N., Kim, H., Koutroulis, A., Liu, J., Papadimitriou, L., Schewe, J., Müller Schmied, H., Stacke, T., Telteu, C.-E., Thiery, W., Veldkamp, T., Zhao, F., and Wada, Y.: Global terrestrial water storage and drought severity under climate change, Nature Climate Change, 11, 226-233, https://doi.org/10.1038/s41558-020-00972-w, 2021.

Qu, Z., Huang, S., Hu, H., Liu, D., Liu, H., and Wang, L.: Climate change and land-use policies exacerbate run-off reduction in a semi-arid inland river basin, Journal of Hydrology, 649, 132396, https://doi.org/10.1016/j.jhydrol.2024.132396, 2025.

Shaik, E. and Fan, D.: Changes in runoff and sediment discharge and their influencing factors in the lower Brahmaputra River, Bangladesh, Journal of Hydrology, 662, 133924, https://doi.org/10.1016/j.jhydrol.2025.133924, 2025.

https://doi.org/10.5194/egusphere-2025-6227
Preprint. Discussion started: 24 February 2026

Sharma, A., Patel, P. L., and Sharma, P. J.: Influence of climate and land-use changes on the sensitivity of SWAT model parameters and water availability in a semi-arid river basin, CATENA, 215, 106298, https://doi.org/10.1016/j.catena.2022.106298, 2022.

Shi, P., Li, P., Li, Z., Sun, J., Wang, D., and Min, Z.: Effects of grass vegetation coverage and position on runoff and sediment yields on the slope of Loess Plateau, China, Agricultural Water Management, 259, 107231, https://doi.org/10.1016/j.agwat.2021.107231, 2022.

Sofokleous, I., Bruggeman, A., Camera, C., and Eliades, M.: Grid-based calibration of the WRF-Hydro with Noah-MP model with improved groundwater and transpiration process equations, Journal of Hydrology, 617, https://doi.org/10.1016/j.jhydrol.2022.128991, 2023.

Sun, Y., Liu, W., Xu, Y., Hou, Y., Zhao, F., and Shen, F.: Quantifying the impacts of climate change and fruit tree expansion on water retention in a sub-tropical watershed, Journal of Cleaner Production, 536, 147146, https://doi.org/10.1016/j.jclepro.2025.147146, 2025.

Tian, L., Guo, S., Feng, J., and He, C.: Quantifying the altitudinal response of water yield capacity to climate change in an alpine basin on the Tibetan Plateau through integrating the WRF-Hydro and Budyko framework, CATENA, 242, 108087, https://doi.org/10.1016/j.catena.2024.108087, 2024.

Towler, E., Foks, S. S., Dugger, A. L., Dickinson, J. E., Essaid, H. I., Gochis, D., Viger, R. J., and Zhang, Y.: Benchmarking high-resolution hydrologic model performance of long-term retrospective streamflow simulations in the contiguous United States, Hydrol. Earth Syst. Sci., 27, 1809-1825, https://doi.org/10.5194/hess-27-1809-2023, 2023.

Turkeltaub, T. and Bel, G.: Changes in mean evapotranspiration dominate groundwater recharge in semi-arid regions, Hydrol. Earth Syst. Sci., 28, 4263-4274, https://doi.org/10.5194/hess-28-4263-2024, 2024.

Van Loon, A. F., Gleeson, T., Clark, J., Van Dijk, A. I. J. M., Stahl, K., Hannaford, J., Di Baldassarre, G., Teuling, A. J., Tallaksen, L. M., Uijlenhoet, R., Hannah, D. M., Sheffield, J., Svoboda, M., Verbeiren, B., Wagener, T., Rangecroft, S., Wanders, N., and Van Lanen, H. A. J.: Drought in the Anthropocene, Nature Geoscience, 9, 89-91, https://doi.org/10.1038/ngeo2646, 2016.

Wang, D., Peng, Q., Li, X., Zhang, W., Xia, X., Qin, Z., Ren, P., Liang, S., and Yuan, W.: A long-term high-resolution dataset of grasslands grazing intensity in China, Scientific Data, 11, 1194, https://doi.org/10.1038/s41597-024-04045-x, 2024.

Wang, L., Li, Y., Biswas, A., Zhao, Y., Niu, B., and Siddique, K. H. M.: Assessing climate change and human impacts on runoff and hydrological droughts in the Yellow River Basin using a machine learning-enhanced hydrological modeling approach, Journal of Environmental Management, 380, 125091, https://doi.org/10.1016/j.jenvman.2025.125091, 2025a.

Wang, L., He, F., Zhao, Y., Wang, J., Lu, P., Jia, Y., Liu, K., Deng, H., and Cui, H.: Inter-basin water transfer will face greater drought risk in the future, Journal of Environmental Management, 385, 125649, https://doi.org/10.1016/j.jenvman.2025.125649, 2025b.

https://doi.org/10.5194/egusphere-2025-6227
Preprint. Discussion started: 24 February 2026

Wang, X., Liu, Z., Jun Xu, Y., Mao, B., and Jia, S.: Extreme drought affects lake water quality, quantity, morphometry: Evidence from China's largest fresh water lake under the 2022 global drought, Geoscience Frontiers, 16, 102146, https://doi.org/10.1016/j.gsf.2025.102146, 2025c.

Wang, X., Dai, Y., Xu, Y. J., Lv, Q., Ji, X., Mao, B., Jia, S., Liu, Z., Luo, C., and Rong, Y.: Dual-quantification of the different contributions of climate change and anthropogenic activities to eutrophication of rivers and lakes in Asia's largest river basin (Yangtze River), Journal of Hazardous Materials, 496, 139205, https://doi.org/10.1016/j.jhazmat.2025.139205, 2025d.

Wang, Y., Hessen, D. O., Samset, B. H., and Stordal, F.: Evaluating global and regional land warming trends in the past decades with both MODIS and ERA5-Land land surface temperature data, Remote Sensing of Environment, 280, 113181, https://doi.org/10.1016/j.rse.2022.113181, 2022a.

Wang, Y., Wang, S., Zhao, W., and Liu, Y.: The increasing contribution of potential evapotranspiration to severe droughts in the Yellow River basin, Journal of Hydrology, 605, 127310, https://doi.org/10.1016/j.jhydrol.2021.127310, 2022b.

Xie, X., Huang, G., Wang, S., Wang, F., and Xie, S.: Interpretable deep learning for dynamic rainfall-runoff prediction: Integrating adaptive signal decomposition and spatiotemporal feature extraction, Journal of Environmental Management, 398, 128444, https://doi.org/10.1016/j.jenvman.2025.128444, 2026.

Yan, D., Zhang, X., Qin, T., Li, C., Zhang, J., Wang, H., Weng, B., Wang, K., Liu, S., Li, X., Yang, Y., Li, W., Lv, Z., Wang, J., Li, M., He, S., Liu, F., Bi, W., Xu, T., Shi, X., Man, Z., Sun, C., Liu, M., Wang, M., Huang, Y., Long, H., Niu, Y., Dorjsuren, B., Gedefaw, M., Li, Y., Tian, Z., Mu, S., Wang, W., and Zhou, X.: A data set of distributed global population and water withdrawal from 1960 to 2020, Scientific Data, 9, 640, https://doi.org/10.1038/s41597-022-01760-1, 2022.

Yan, Y., Liu, Z., Chen, L., Chen, X., Lin, K., Zeng, Z., Lan, X., Huang, L., Wang, Y., Yao, L., Cheng, L., and Ma, Z.: Earth greening and climate change reshaping the patterns of terrestrial water sinks and sources, Proceedings of the National Academy of Sciences, 122, e2410881122, https://doi.org/10.1073/pnas.2410881122, 2025.

Yang, Z., Niu, G., Mitchell, K. E., Chen, F., Ek, M. B., Barlage, M., Longuevergne, L., Manning, K., Niyogi, D., Tewari, M., and Xia, Y.: The community Noah land surface model with multiparameterization options (Noah-MP): 2. Evaluation over global river basins, Journal of Geophysical Research: Atmospheres, 116, https://doi.org/10.1029/2010JD015140, 2011.

Yao, L., Zhang, J., Cao, C., and Zheng, F.: Parameter estimation and uncertainty quantification of rainfall-runoff models using data assimilation methods based on deep learning and local ensemble updates, Environmental Modelling & Software, 185, 106332, https://doi.org/10.1016/j.envsoft.2025.106332, 2025.

Yu, E., Liu, X., Li, J., and Tao, H.: Calibration and Evaluation of the WRF-Hydro Model in Simulating the Streamflow over the Arid Regions of Northwest China: A Case Study in Kaidu River Basin, Sustainability, 15, 6175, https://doi.org/10.3390/su15076175, 2023.

Zhang, G., Tang, D., Li, S., Fan, Y., Pulatov, A., Sun, A., Qi, X., Wang, L., and Li, Y.: Climate and land use regulate vegetation–runoff interaction pathways in the three-river source region, Journal of Environmental Management, 393, 127127, https://doi.org/10.1016/j.jenvman.2025.127127, 2025.

https://doi.org/10.5194/egusphere-2025-6227
Preprint. Discussion started: 24 February 2026

555 Zhou, Y., Batelaan, O., Guan, H., Duan, L., Liu, T., Wang, Y., Li, X., and Yang, B.: Evaluation of the contributions of climate change and overgrazing to runoff in a typical grassland inland river basin, Journal of Hydrology: Regional Studies, 52, 101725, https://doi.org/10.1016/j.ejrh.2024.101725, 2024.